AGU PUBLICATIONS

Geophysical Research Letters

RESEARCH LETTER
10.1002/2017GL073733

Key Points:
- Climate model simulations show distinct hot spots, robust across most CMIP5 models, where daily hot extremes warm faster than mean temperatures
- Changes in surface energy fluxes, consistent with drying soils, accelerate warming on the day hot extremes occur
- The spatial patterns of accelerated warming of hot extremes in the CMIP5 models are inconsistent with observations, except over Europe

Supporting Information:
- Supporting Information S1

Correspondence to:
M. G. Donat,
m.donat@unsw.edu.au

Citation:
Donat, M. G., A. J. Pitman, and S. I. Seneviratne (2017), Regional warming of hot extremes accelerated by surface energy fluxes, *Geophys. Res. Lett.*, *44*, 7011–7019, doi:10.1002/2017GL073733.

Received 4 APR 2017
Accepted 22 JUN 2017
Accepted article online 11 JUL 2017
Published online 15 JUL 2017

Regional warming of hot extremes accelerated by surface energy fluxes

M. G. Donat[1], A. J. Pitman[1], and S. I. Seneviratne[2]

[1]Climate Change Research Centre and ARC Centre of Excellence for Climate System Science, UNSW, Sydney, New South Wales, Australia, [2]Institute for Atmospheric and Climate Science, Department of Environmental Systems Science, ETH Zurich, Zurich, Switzerland

Abstract Strong regional differences exist in how hot temperature extremes increase under global warming. Using an ensemble of coupled climate models, we examine the regional warming rates of hot extremes relative to annual average warming rates in the same regions. We identify hot spots of accelerated warming of model-simulated hot extremes in Europe, North America, South America, and Southeast China. These hot spots indicate where the warm tail of a distribution of temperatures increases faster than the average and are robust across most Coupled Model Intercomparison Project Phase 5 models. Exploring the conditions on the specific day when the hot extreme occurs demonstrates that the hot spots are explained by changes in the surface energy fluxes consistent with drying soils. However, the model-simulated accelerated warming of hot extremes appears inconsistent with observations, except over Europe. The simulated acceleration of hot extremes may therefore be unreliable, a result that necessitates a reevaluation of how climate models resolve the relevant terrestrial processes.

1. Introduction

As the Earth's climate warms, the temperatures associated with hot temperature extremes have also increased [*Hartmann et al.,* 2013] and are very likely to continue to increase into the future [*Collins et al.,* 2013]. Observations and climate models both show that the spatial patterns of changes in hot temperatures vary regionally, with locally different warming rates [*Donat et al.,* 2013b; *Sillmann et al.,* 2013]. Most recently, *Seneviratne et al.* [2016] used an ensemble of models to demonstrate that regional increases in temperature extremes can differ substantially from the global average temperature increases and in particular that hot extremes are increasing by more than the global average temperature in some important land regions. These regional increases in hot extremes can have very large implications [*Vasseur et al.,* 2014] and far more societal impact than implied by global average temperature changes [*Intergovernmental Panel on Climate Change*, 2012].

Observed increases in the temperature of hot extremes are largest in some Northern Hemisphere midlatitude regions including Western Europe, the Mediterranean, high-latitude regions of North America, western and eastern Australia, and regions of eastern Russia [*Donat et al.,* 2013b]. Regional differences in warming rates of hot extremes have been documented therefore, but the physical mechanisms that explain the regional patterns and why extremes increase by more than the global average in some, but not all, regions remain to be fully explained.

Different physical mechanisms drive regional increases in hot temperatures in different regions. In many regions, local annual average temperature increases seem to be the main driver of increases in hot extremes. In these circumstances, the whole temperature distribution shifts toward warmer conditions [*Donat and Alexander*, 2012; *Rhines and Huybers*, 2013; *Lewis and King*, 2017]. This increases the probability of hot extremes but does not accelerate increases in hot extremes relative to the average. The annual average temperature warming rates are higher over most land areas than over the ocean, and strongest in high latitude and midlatitude regions of the northern hemisphere [*Hartmann et al.,* 2013], and may explain some of the regional differences in the warming of hot extremes. Some regions, however, show disproportionate warming rates of hot extremes compared to annual average temperatures. This includes regions where increases in hot extremes accelerate relative to the average, implying a change in the shape of the distribution and pointing to other mechanisms that locally amplify changes in extremes relative to average temperature changes. These mechanisms could include changes in dynamics or thermodynamics leading to conditions more conducive to increased hot extremes. For example, several studies point to the midlatitudes as being regions where hot extremes increase strongly as a consequence of soil moisture feedbacks [*Seneviratne et al.,* 2006, 2013;

Diffenbaugh and Ashfaq, 2010; *Hirschi et al.,* 2011; *Lorenz et al.,* 2016]. Additional evidence suggests that soil moisture feedbacks are instrumental in explaining why hot extremes are increasing faster than the global average [*Berg et al.,* 2016; *Vogel et al.,* 2017]. Further mechanisms that have been investigated include changes in the atmospheric circulation, such as atmospheric blocking [*Fischer and Schär*, 2010] which has been associated with increases in European heatwaves [*Klein Tank and Können*, 2003; *Horton et al.,* 2015]. Changes in advection of heat can also amplify hot extremes relative to the averages [*Miralles et al.,* 2014]. Changes in atmospheric processes including cloud cover and the associated feedbacks on incoming solar radiation and net long wave radiation can trigger increases in hot extremes, amplified by changes in specific land surface states and feedbacks [*Seneviratne et al.,* 2010; *Lorenz et al.,* 2013; *Hauser et al.,* 2016] all interwoven with changes in atmospheric dynamics [*Cattiaux et al.,* 2013].

Building on these previous studies, our paper has three novel aspects. First, previous studies have examined accelerated warming in hot extremes relative to a global annual temperature average change in the context of climate projections [*Seneviratne et al.,* 2016; *Vogel et al.,* 2017]. In this paper, we explore, for the first time, where and why hot temperature extremes are increasing by more than expected from the increase in the local annual average temperature. If global warming were spatially uniform, the use of global average temperature would be all that was necessary. However, a given increase in the global average temperature leads to some regions with far higher and some with lower average warming than the global average. We therefore build on *Seneviratne et al.* [2016] by using local model-specific changes in annual average temperature and identify regions where the change in the temperature distribution is focussed on the tail, not just on an overall shift as reflected by the average change. A second novel aspect of our study is its focus on the conditions on the hottest day, whereas previous studies have associated extreme temperatures with conditions averaged over several months [*Vogel et al.,* 2017]. We are interested in the annual hottest day simulated by each of the Coupled Model Intercomparison Project Phase 5 (CMIP5) models, and how this changes in the future. We therefore examine the conditions on the actual day that the annual hottest day occurs for a given location. We then examine whether changes in the partitioning of net radiation between latent and sensible heat fluxes help explain why the very hot day warmed by more than implied by the local change in the average. This approach focuses more closely on the physical processes that cause the changes, rather than inferring plausible explanations of daily extremes from monthly or seasonal average conditions. Our goal is to examine whether changes in these fluxes help explain the amplification of hot extremes, relative to local average temperature changes, on the specific day in question. As a third novel aspect, we analyze the modeled and observed tendencies in changes of the temperatures in the warm tails compared with the average of the temperature distributions to assess where and whether observations confirm the overall tendencies projected by climate models.

2. Data and Methods

We use climate model simulations from the CMIP5 archive [*Taylor et al.,* 2012] to investigate changes in average and extreme temperatures, and we associate these with changes in the simulated latent and sensible heat fluxes on the specific day the hot extreme occurs. We use data from the historical runs combined with simulations following the Representative Concentration Pathway 8.5 (RCP8.5) scenario to investigate changes from the midtwentieth century until the end of the 21st century. We restrict the analysis to after 1950 because daily sensible and latent heat fluxes were only available from some CMIP5 models after this year. We chose the RCP8.5 scenario because the absolute warming is largest in this scenario, allowing clearer signals to be identified. We note that scaling rates of both local average and extreme temperatures relative to global average temperature increases were found to be insensitive to different emission scenarios [*Seneviratne et al.,* 2016]. Our findings are therefore likely robust to the choice of specific emission scenarios. We used data from 25 CMIP5 models (ACCESS1-0, ACCESS1-3, bcc-csm1-1, BNU-ESM, CanESM2, CCSM4, CMCC-CESM, CNRM-CM5, CSIRO-Mk3-6-0, GFDL-CM3, GFDL-ESM2G, GFDL-ESM2M, HadGEM2-CC, HadGEM2-ES, inmcm4, IPSL-CM5A-LR, IPSL-CM5A-MR, IPSL-CM5B-LR, MIROC5, MIROC-ESM, MIROC-ESM-CHEM, MPI-ESM-LR, MPI-ESM-MR, MRI-CGCM3, NorESM1-M), from most models we used the simulation r1i1p1, and only from CCSM4 we used r6i1p1. The choice of models was determined by availability of the required daily variables for the historical and RCP8.5 simulations. We use a single simulation from each CMIP5 climate model to ensure equal weighting of all models in the ensemble averages, but we do not consider model independence [e.g., *Abramowitz and Bishop*, 2015].

From each model simulation we use monthly average temperatures (*tas*) to calculate the local annual average temperature (T_{mean}) change. The annually hottest day (TXx) is determined from daily maximum temperatures (variable name *tasmax*). Most CMIP5 models did not record soil moisture as a daily output variable, and so we cannot explore the change in daily soil moisture associated with TXx. However, soil moisture is not a variable communicated by the land surface to the atmosphere; rather, it is used to control the partitioning of net radiation between the latent and sensible heat fluxes, which are then communicated to the atmosphere. We therefore use the partitioning of latent and sensible heat fluxes (variable names *hfls* and *hfss*) as a proxy for soil moisture when investigating conditions on the specific days when TXx occurs. We calculate the evaporative fraction EF from latent (Q_e) and sensible (Q_h) heat fluxes as EF = $Q_e/(Q_e + Q_h)$ to characterize the partitioning of net radiation between these fluxes. We use EF rather than the Bowen Ratio ($\beta = Q_h/Q_e$) because β can become unbounded in very dry conditions when Q_e tends toward zero.

All model fields are remapped to a common 2.5° × 2.5° grid using a first-order conservative remapping technique [*Jones*, 1999] to enable combining data from the different models into ensemble averages. We focus on extreme temperature and related heat flux changes over land and therefore mask out all nonland grid points.

At each grid box, we determine TXx as the annual maximum of *tasmax* and record the date when this maximum occurs. We then select Q_e and Q_h for that specific day. As TXx may occur on different days at different grid points, the TXx, Q_e and Q_h fields are not necessarily spatially continuous and may reflect different days, but TXx, Q_e, and Q_h are always compared with each other on the same day.

To compare modeled and observed temperature changes, we use gridded TXx fields from the HadEX2 [*Donat et al.,* 2013b] and GHCNDEX [*Donat et al.,* 2013a] data sets and gridded monthly mean temperature fields from the HadCRUT4 data set [*Morice et al.,* 2012]. We merged the HadEX2 and GHCNDEX data sets following *Dittus et al.* [2015] to obtain the best possible spatial coverage of observed temperature extremes. The HadCRUT4 data set consists of an ensemble of 100 realizations that account for measurement and sampling errors and coverage uncertainty. We use the median of these 100 ensemble members, calculated at each grid box. The comparison of the observational temperature data sets is performed at the 3.75° × 2.5° grid of the HadEX2 data set, which is the coarsest grid of the three observational products. The data sets with higher resolution were remapped to this grid using a first-order conservative remapping technique [*Jones*, 1999].

3. Results

To identify regions where hot extremes warm at a different rate compared to local annual average temperatures, we derive the ratio of TXx relative to T_{mean} changes at each location. The CMIP5 future projections show hot spots where the TXx increases faster than the local annual T_{mean} (regions in Figure 1a where ratios exceed 1.0). Hot spots of accelerated warming of hot extremes relative to the local annual average are notable over Europe, the contiguous United States, and South America. To a smaller extent, accelerated warming of hot extremes is also found in some regions of Southeast China, Southeast Asia, northern and southern Africa, and southern Australia. Areas where hot extremes are projected to warm more slowly than annual average temperatures are almost entirely constrained to the high northern latitudes of North America and northern Asia. In these regions, strongest warming is observed and simulated during winter [*Screen and Simmonds*, 2013], which dominates the annual average temperature increases, while warming in summer (when the hottest days occur) is comparably small.

These patterns of amplification of TXx relative to annual T_{mean} are a robust feature across most individual CMIP5 models (supporting information Figure S1). More than 20 out of the 25 CMIP5 models display this amplification in central and southern Europe (and none of the models has warming ratios less than 1 in southern Europe). Similarly, for the contiguous United States and large areas in South America, more than 80% of CMIP5 models indicate TXx increases at a higher rate than T_{mean}.

We note that seasonal average temperature changes may be different to changes in annual average temperature. Indeed, changes in hot extremes may be more closely related to changes in average summer temperatures [*Orlowsky and Seneviratne,* 2012; *Argüeso et al.,* 2016]. We therefore also compared the rates of changes in hot extremes with seasonal average temperature changes, averaged over the months when hot extremes usually occur in extratropical regions of the northern (June-July-August) and southern (December-January-February) hemisphere (supporting information Figure S2). All hot spots of accelerated

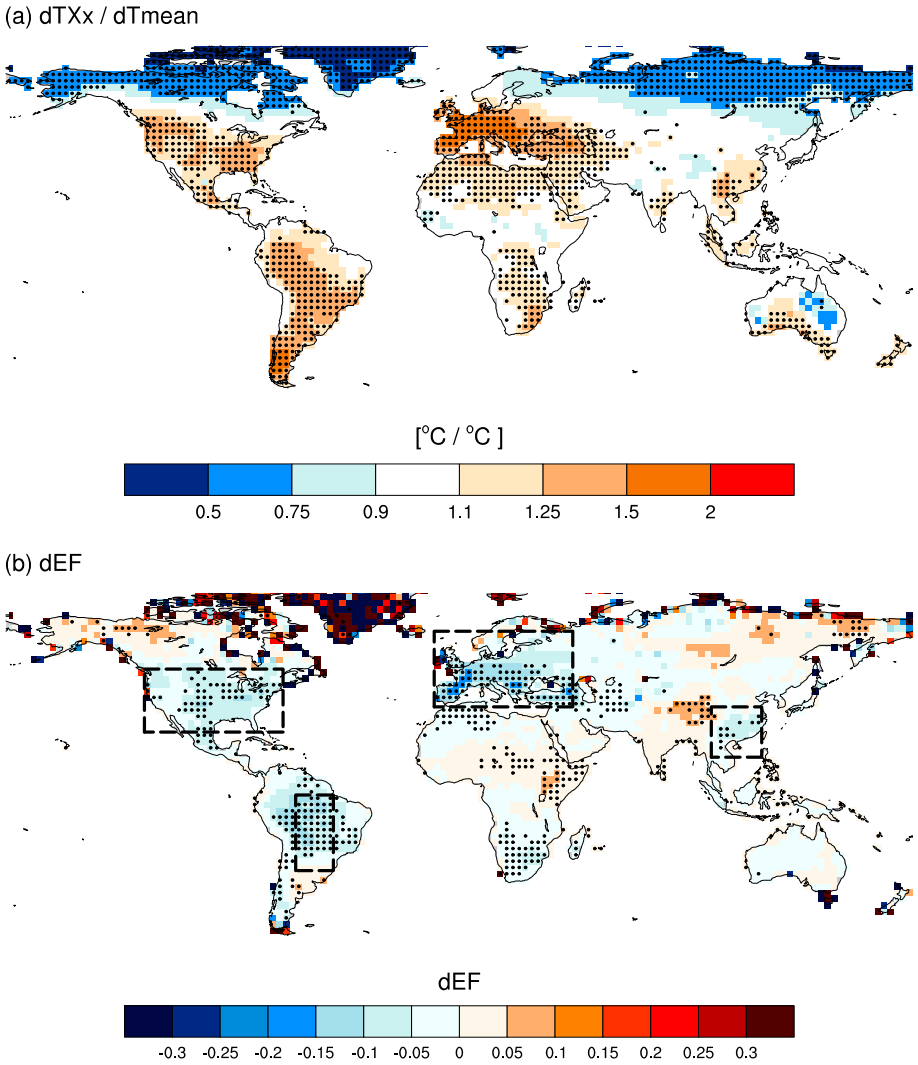

Figure 1. (a) CMIP5 ensemble average change in the temperature of the annually hottest day (TXx) relative to the change in local annual average temperatures, (b) and the evaporative fraction (EF) on the annually hottest day, both between the midtwentieth century (1951–1980) average and the late 21st century (2070–2099) average. Stippling indicates where at least 20 models (out of 25) simulate scaling rates above one or below one (Figure 1a), or agree on the sign of change (Figure 1b). Dashed boxes indicate regions used for further analysis in Figure 2.

warming are still apparent when comparing dTXx to the warming of warm season average temperatures, although over Europe and North America they are somewhat weaker relative to the annual average. In these two regions, summer average temperatures also show accelerated warming compared to annual average temperatures, and therefore, summer warming generally contributes to the accelerated warming of hot extremes relative to annual average temperatures in Europe and North America. This is not the case in other regions of accelerated warming (southeast China, South America, South Africa, and southern Australia) where summer temperatures do not rise faster than annual average temperatures. Comparing TXx changes to seasonal average temperature changes therefore leads to mostly similar results to comparing with annual average temperature changes.

Figure 1b shows the ensemble average change in EF on the day that TXx occurs. The CMIP5 ensemble average shows large-scale reductions in EF over the same regions where hot spots of accelerated warming of hot extremes occur in the future projections (Figure 1b). This similarity between the TXx amplification hot spots (Figure 1a) and the regions with largest reductions in the EF is also found in most individual models (supporting information Figure S3). This suggests that the finding that amplified warming of hot extremes is related to reduced evaporative cooling is a robust feature across the majority of CMIP5 models and occurs in similar

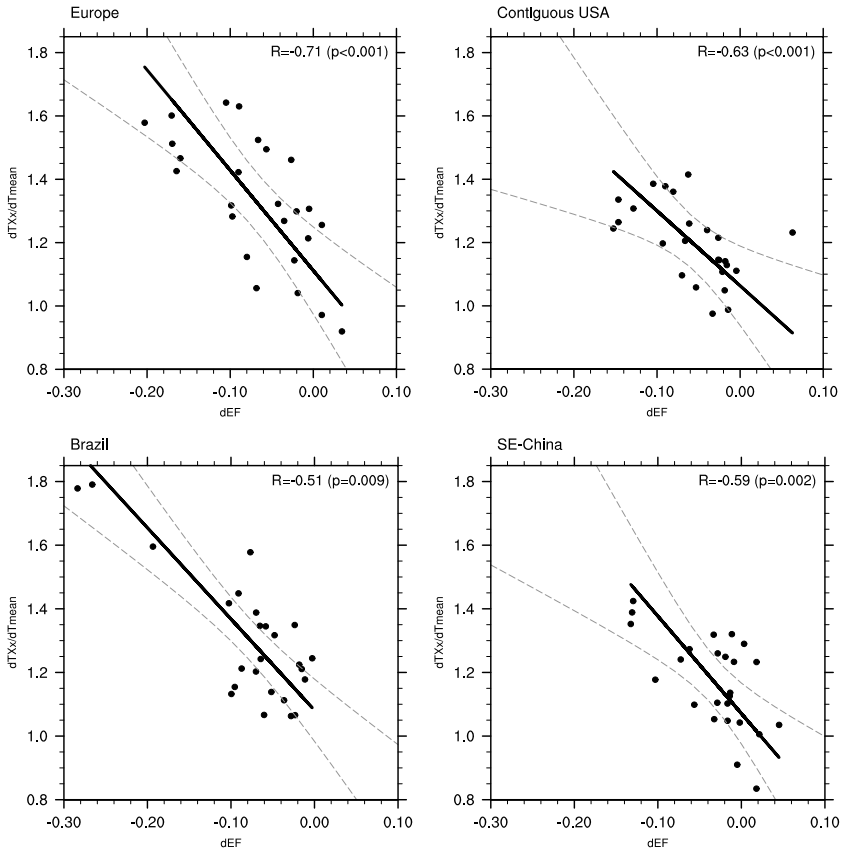

Figure 2. Scatterplot showing the change in evaporative fraction on the day of TXx (dEF, *x* axis) and the change in TXx relative to the local average temperature change (dTXx/dT_{mean}, *y* axis) for the different models in the four hot spot regions (see boxes in Figure 1b). Temperature and evaporative fraction changes were calculated between the midtwentieth century (1951–1980) and the late 21st century (2070–2099). Each dot represents one model simulation. Solid black lines show the total least squares regression between dEF and dTXx/dT_{mean}, gray dashed lines show the 95% confidence interval of the regression function based on 1000 bootstraps, and *R* is the Spearman's rank correlation between both variables including the *p* value of the correlation.

regions in most models. Although most CMIP5 models broadly agree on the regions where the strongest amplification of hot extremes occur, the magnitude of the dTXx/dT_{mean} ratio and the magnitude of the change in EF differs between the individual CMIP5 models.

If the cause of the stronger warming in TXx in those "hot spot" regions of Figure 1a is related to changes in the partitioning of net radiation between Q_e and Q_h (Figure 1b), there should be a correlation between TXx and EF on the day that the hottest temperatures occur. Figure 2 (a scatterplot of the results displayed in Figures 1a and 1b for four hot spot regions) shows the model-specific magnitude of the change in TXx relative to the change in T_{mean} against the magnitude of the EF changes. Models where the EF decreases most strongly also show a stronger amplification of hot extremes in all four hot spot regions. However, Figure 2 also shows that the model-specific change in EF, and the change in TXx relative to T_{mean}, varies widely amongst the CMIP5 models.

The future projected amplification of heat extremes is also related to the strength of correlation in the current climate between the temperature of the annually hottest day and partitioning of Q_e and Q_h on that day. That is, regions that are characterized by a stronger relationship between TXx and EF in the current climate also experience a stronger amplification of TXx relative to T_{mean} in the future projections. We calculated the correlation, over the past 60 years, between TXx and EF as a measure of coupling strength between soil moisture and the temperature extremes under current climate conditions. In most models, the regions where we find accelerated warming in TXx in the future projections (supporting information Figure S1) are characterized by statistically significant ($p < 0.05$) anticorrelations between TXx and EF (supporting information Figure S4).

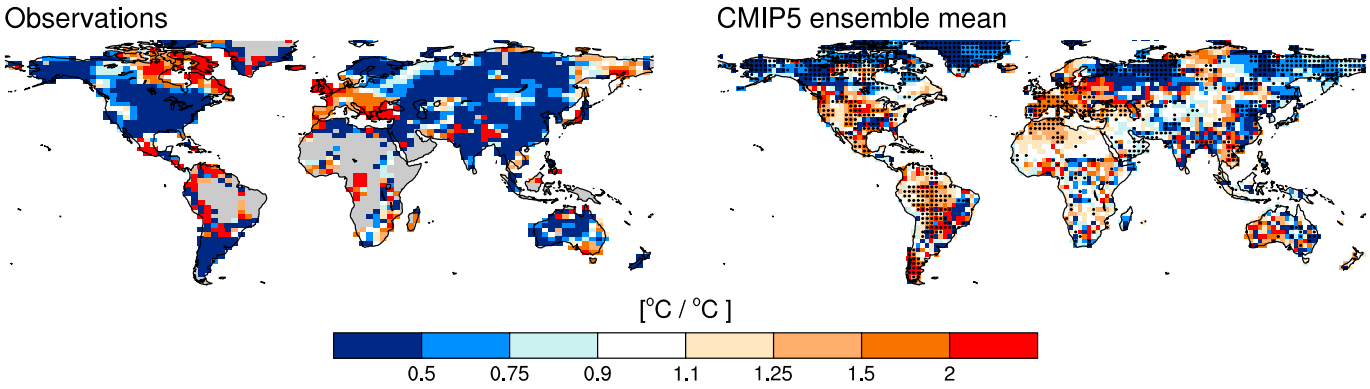

Figure 3. Recent changes in extreme temperatures (TXx) relative to the change in local average temperatures between the midtwentieth century (1951–1980) and the late 20th/early 21st century (1981–2010). (left) Based on observational data (TXx from HadEX2 and GHCNDEX merged and T_{mean} from HadCRUT); (right) CMIP5 ensemble average. Stippling indicates where at least two thirds of the models (i.e., 17 out of 25) simulate scaling rates above one or below one.

This means that in these hot spot regions where we see strongest amplification in the future projections are also regions that are characterized by a strong relationship between EF and TXx in the current climate. We further examine the relationship of these TXx-EF correlations under recent climate conditions with the amplification of hot extremes in the future climate projections in the four hot spot regions (supporting information Figure S5). We find statistically significant ($p < 0.05$) relationships over Europe, the contiguous United States, and southeast China with anticorrelations between -0.48 and -0.6. These relationships point to a potential emergent constraint [*Klein and Hall*, 2015] for regional hot extremes. Models that are characterized by strong anticorrelations between EF and temperature of the hottest day in the recent climate show the strongest future accelerated warming of hot extremes, and vice versa. However, due to the lack of global long-term, high-quality observations of surface heat fluxes or soil moisture, it is currently hard to assess which of the models demonstrate realistic behavior under recent climate conditions.

Our results from the CMIP5 models are therefore reasonably robust; conclusions reached from the ensemble average are supported by the majority of individual models, and there is a consistency across models in the relationships that explain the scaling of TXx. Where the scaling of TXx is strongest relative to the average at a given location, we find the strongest decreases in EF. This points to low Q_e being coincident with the amplifications of TXx relative to T_{mean} and as discussed by *Vogel et al.* [2017] suggests drying soils as the likely cause.

The question is whether this consistent behavior in the CMIP5 models is supported by observations. We therefore compare the scaling rates of TXx to changes in T_{mean} derived from the CMIP5 models to observational data. We focus on the period 1951–2010 when observations are most complete, and calculate TXx differences and T_{mean} differences between the averages of the two 30 year periods 1951–1980 and 1981–2010. The CMIP5 model-simulated scaling rates over this shorter period (Figure 3b) are qualitatively similar to the simulated changes until the late 21st century (Figure 1a) and show hot spots of accelerated warming in TXx in similar locations. Due to the smaller signal-to-noise ratio on shorter time scales, the spatial patterns are understandably noisier over the 60 year period as compared to the future projected changes through to the end of the 21st century.

Observations (Figure 3a) show accelerated warming of TXx over much of Europe, consistent with the CMIP5 simulations. However, observed scaling rates over most of North America are smaller than one, indicating that extreme temperatures are changing at a slower rate than average temperatures. This is consistent with the "warming hole" over the eastern U.S. [*Portmann et al.,* 2009] where summer temperatures have not increased, and the observed hottest days show slight cooling trends over the past century [*Donat et al.,* 2013b]. One possible explanation might be related to the increased use of regional irrigation [*Mueller et al.,* 2015]. In regions along the west coast, where average and extreme temperatures have been observed to increase, the warming rate of TXx is generally lower than the warming of T_{mean}. Over large parts of South America reliable observations are unavailable. However, over the southern tip of South America, where we have observations, we also find observed scaling rates smaller than one, inconsistent with CMIP5 simulations. Observations also do not show a hot spot of accelerated warming over southeast China, although some small

areas with accelerated warming of hot extremes are found over eastern South America, southern Africa, and southeast Australia.

We note that of the 25 model simulations analyzed here, a few models simulate a scaling smaller than one over extended areas of North America (supporting information Figures S6 and S7, e.g., MPI-LSM-LR and CNRM-CM5). This suggests that it is possible that the lack of amplified warming in the observations may in part be explained by internal climate variability. However, in these simulations where scaling over North America looks somewhat similar to observations, the scaling over other regions such as South America or Europe by the same models is different to observations. This underlines the need for a comprehensive process-based evaluation of modeled and observed changes in hot extremes relative to average temperatures in the different regions. In order to provide reliable information about future amplification of hot extremes, models would be expected to be consistent with observations concurrently in all regions.

4. Discussion and Conclusions

CMIP5 models simulate patterns of accelerated warming in TXx relative to T_{mean} over Europe, the United States, South America, southeast China, and parts of Southern Africa and southern Australia. These changes are related to the partitioning of surface energy fluxes and reflect a lower Q_e and a higher Q_h on the specific days when TXx occurs. This is likely related to soil moisture feedbacks; under drier conditions less evaporative cooling leads to amplified warming of the hottest days.

The regions where the CMIP5 models simulate patterns of accelerated warming in TXx relative to T_{mean} are robust across most of the CMIP5 models. Our results suggest that the global patterns of where extremes warm at higher rates than local averages can be explained by a decrease in the EF on the day when the hot extreme occurs. The lack of reported soil moisture on daily timescales from CMIP5 models prevents us from demonstrating that soil moisture changes cause the declines in EF; however, physical reasoning and existing literature strongly suggests that soil moisture's control on the partitioning of net radiation at the surface explains the change in EF.

There is an alternative potential explanation for our results linked with changes in clouds, incoming solar radiation, and their interactions with soil moisture [e.g., *Boé and Terray*, 2008]. We explored the changes in incoming solar radiation and changes in total cloud cover and found a less consistent relationship between the hot spot regions and changes in these variables. This is not definitive; the day when TXx occurs may be the result of a series of days with very high solar forcing under conditions of synoptic blocking and a strong land-atmosphere feedback heating the boundary layer [e.g., *Miralles et al.,* 2014]. On the day that TXx occurs more cloud could limit outgoing infrared radiation and combine with the accumulated heat to further warm the surface and lead to the hottest temperature. The lack of a consistent pattern of increased solar radiation with TXx is therefore not proof that these forcings do not drive TXx, but our analysis points to the change in EF being the dominant driver of TXx on the day in question. Further analyses that decompose all the energy components on the day that TXx occurs and combines this with EF and explores these over several days leading up to the day TXx occurs would be valuable. This could be combined with an analysis of synoptic patterns [e.g., *Gibson et al.,* 2016] and advection of heat.

Our finding that the CMIP5 simulated patterns of accelerated warming are potentially inconsistent with available observations over North America, China, and elsewhere where we have observations is concerning. That is, apart from Europe, most of those hot spot regions highlighted previously are not supported by observational evidence. The majority of published analyses linking temperature extremes to soil moisture feedbacks are focused on Europe, and our results support these studies, but our results also raise questions as to how generalizable these results might be. Based on the limited evidence available, we suggest that the CMIP5 models cannot currently simulate the observed spatial patterns of changes in hot extremes where these relate to amplification through EF. Since they do not correctly simulate the observed period for $dTXx/dT_{mean}$ (Figure 3), we suggest the CMIP5 models may not be reliable in projecting changes in TXx in the future in several regions. However, based on CMIP5 simulations, comparisons with observations (Figure 3) and a large body of previous work our results do support strong soil-moisture temperature feedbacks over Europe as a potential amplifier of CO_2-induced warming.

Efforts to improve climate models to better capture the real-world changes in hot extremes are needed to enable more reliable future projections. Soil moisture appears to be the key to understanding how temperature extremes scale with temperature averages. Soil moisture is the result of multiple interacting processes, starting with rainfall. As noted by *Marotzke et al.* [2017], and discussed by *Bony et al.* [2015], changes in rainfall patterns are strongly linked to changes in the circulation of the atmosphere and oceans but how these are expressed on regional scales remains poorly understood. What seems increasingly apparent though is to capture these regional changes, and associated extreme events such as heat waves, climate models will have to utilize far higher spatial resolution [*Palmer*, 2014; *Marotzke et al.,* 2017]. If rainfall is simulated well, then how the land surface partitions net radiation between the sensible and latent heat fluxes is important since these fluxes feedback through the atmospheric boundary layer and can exacerbate heat waves [*Miralles et al.,* 2014] and temperature extremes. These, in turn, depend on the availability of soil moisture on the days when the synoptic conditions are conducive to extreme temperatures [*Miralles et al.,* 2012; *Quesada et al.,* 2012]. A further important contribution to the identified discrepancies may be the role of changes in land management. One recent study suggests that the cooling of heat extremes observed in the eastern United States could be related to cropping and associated irrigation [*Mueller et al.,* 2015]. Irrigation was not considered in the CMIP5 ensemble but could induce a substantial cooling in simulated hot extremes in some regions if of sufficient scale [*Thiery et al.,* 2017].

Without observations focused on the processes that link soil moisture, evaporative fraction, and atmospheric feedbacks on very hot days we cannot fully assess the seriousness of the mismatch in regions other than Europe, between modeled and observed scaling rates. However, the apparent contradiction over most regions previously identified as hot spots between available observations and the CMIP5 models should act as a serious warning to those using results from these models to project changes in future temperature extremes that occur on short timescales of a few days.

Acknowledgments
This study was supported through the Australian Research Council grants CE110001028 and DE150100456. S.I.S. acknowledges support from the European Research Council (ERC) through the European Community's Seventh Framework Programme (grant agreement FP7-IDEAS-ERC-617518). We thank the climate modeling groups contributing to CMIP5 for producing and making available their model output. CMIP5 data were obtained from the Australian node of the Earth System Grid Federation (ESGF), hosted at the National Computing Infrastructure (NCI). HadCRUT4 monthly temperature fields are provided at http://www.metoffice.gov.uk/hadobs/hadcrut4/. HadEX2 and GHCNDEX extreme temperature data can be obtained from www.climdex.org.

References

Abramowitz, G., and C. H. Bishop (2015), Climate model Dependence and the ensemble Dependence transformation of CMIP projections, *J. Clim.*, *28*(6), 2332–2348, doi:10.1175/JCLI-D-14-00364.1.

Argüeso, D., A. Di Luca, S. E. Perkins-Kirkpatrick, and J. P. Evans (2016), Seasonal mean temperature changes control future heat waves, *Geophys. Res. Lett.*, *43*, 7653–7660, doi:10.1002/2016GL069408.

Berg, A., et al. (2016), Land–atmosphere feedbacks amplify aridity increase over land under global warming, *Nat. Clim. Change*, *6*(9), 869–874, doi:10.1038/nclimate3029.

Boé, J., and L. Terray (2008), Uncertainties in summer evapotranspiration changes over Europe and implications for regional climate change, *Geophys. Res. Lett.*, *35*, L05702, doi:10.1029/2007GL032417.

Bony, S., et al. (2015), Clouds, circulation and climate sensitivity, *Nat. Geosci.*, *8*(4), 261–268, doi:10.1038/ngeo2398.

Cattiaux, J., H. Douville, and Y. Peings (2013), European temperatures in CMIP5: Origins of present-day biases and future uncertainties, *Clim. Dyn.*, *41*(11–12), 2889–2907, doi:10.1007/s00382-013-1731-y.

Collins, M., et al. (2013), *Long-Term Climate Change: Projections, Commitments and Irreversibility*, edited by P. M. Stocker et al., pp. 1029–1136, Cambridge Univ. Press, Cambridge, U. K.

Diffenbaugh, N. S., and M. Ashfaq (2010), Intensification of hot extremes in the United States, *Geophys. Res. Lett.*, *37*, L15701, doi:10.1029/2010GL043888.

Dittus, A. J., D. J. Karoly, S. C. Lewis, and L. V. Alexander (2015), A Multiregion Assessment of observed changes in the areal extent of temperature and precipitation extremes, *J. Clim.*, *28*(23), 9206–9220, doi:10.1175/JCLI-D-14-00753.1.

Donat, M. G., and L. V. Alexander (2012), The shifting probability distribution of global daytime and night-time temperatures, *Geophys. Res. Lett.*, *39*, L14707, doi:10.1029/2012GL052459.

Donat, M. G., L. V. Alexander, H. Yang, I. Durre, R. Vose, and J. Caesar (2013a), Global land-based datasets for monitoring climatic extremes, *Bull. Am. Meteorol. Soc.*, *94*(7), 997–1006, doi:10.1175/BAMS-D-12-00109.1.

Donat, M. G., et al. (2013b), Updated analyses of temperature and precipitation extreme indices since the beginning of the twentieth century: The HadEX2 dataset, *J. Geophys. Res. Atmos.*, *118*, 2098–2118, doi:10.1002/jgrd.50150.

Fischer, E. M., and C. Schär (2010), Consistent geographical patterns of changes in high-impact European heatwaves, *Nat. Geosci.*, *3*(6), 398–403, doi:10.1038/ngeo866.

Gibson, P. B., P. Uotila, S. E. Perkins-Kirkpatrick, L. V. Alexander, and A. J. Pitman (2016), Evaluating synoptic systems in the CMIP5 climate models over the Australian region, *Clim. Dyn.*, *47*(7–8), 2235–2251, doi:10.1007/s00382-015-2961-y.

Hartmann, D. J., et al. (2013), Observations: Atmosphere and surface, in *Climate Change 2013: The Physical Science Basis. Contribution of Working Group I to the Fifth Assessment Report of the Intergovernmental Panel on Climate Change*, edited by P. M. Stocker et al., pp. 159–254, Cambridge Univ. Press, Cambridge, U. K.

Hauser, M., R. Orth, and S. I. Seneviratne (2016), Role of soil moisture versus recent climate change for the 2010 heat wave in western Russia, *Geophys. Res. Lett.*, *43*, 2819–2826, doi:10.1002/2016GL068036.

Hirschi, M., S. I. Seneviratne, V. Alexandrov, F. Boberg, C. Boroneant, O. B. Christensen, H. Formayer, B. Orlowsky, and P. Stepanek (2011), Observational evidence for soil-moisture impact on hot extremes in southeastern Europe, *Nat. Geosci.*, *4*(1), 17–21, doi:10.1038/ngeo1032.

Horton, D. E., N. C. Johnson, D. Singh, D. L. Swain, B. Rajaratnam, and N. S. Diffenbaugh (2015), Contribution of changes in atmospheric circulation patterns to extreme temperature trends, *Nature*, *522*(7557), 465–469, doi:10.1038/nature14550.

Intergovernmental Panel on Climate Change (2012), *Managing the Risks of Extreme Events and Disasters to Advance Climate Change Adaptation*, edited by P. M. Field et al., 582 pp., Cambridge Univ. Press, Cambridge, U. K.

Jones, P. W. (1999), First- and second-order conservative remapping schemes for grids in spherical coordinates, *Mon. Weather Rev.*, *127*(9), 2204–2210, doi:10.1175/1520-0493(1999)127<2204:FASOCR>2.0.CO;2.

Klein, S. A., and A. Hall (2015), Emergent constraints for cloud feedbacks, *Curr. Clim. Change Rep.*, *1*(4), 276–287, doi:10.1007/s40641-015-0027-1.

Klein Tank, A. M. G., and G. P. Können (2003), Trends in indices of daily temperature and precipitation extremes in Europe, 1946–99, *J. Clim.*, *16*(22), 3665–3680, doi:10.1175/1520-0442(2003)016<3665:TIIODT>2.0.CO;2.

Lewis, S. C., and A. D. King (2017), Evolution of mean, variance and extremes in 21st century temperatures, *Weather Clim. Extrem.*, *15*, 1–10, doi:10.1016/j.wace.2016.11.002.

Lorenz, R., E. L. Davin, D. M. Lawrence, R. Stöckli, and S. I. Seneviratne (2013), How important is vegetation phenology for European climate and heat waves?, *J. Clim.*, *26*(24), 10,077–10,100, doi:10.1175/JCLI-D-13-00040.1.

Lorenz, R., et al. (2016), Influence of land-atmosphere feedbacks on temperature and precipitation extremes in the GLACE-CMIP5 ensemble, *J. Geophys. Res. Atmos.*, *121*, 607–623, doi:10.1002/2015JD024053.

Marotzke, J., et al. (2017), Climate research must sharpen its view, *Nat. Clim. Change*, *7*(2), 89–91, doi:10.1038/nclimate3206.

Miralles, D. G., M. J. van den Berg, A. J. Teuling, and R. A. M. de Jeu (2012), Soil moisture-temperature coupling: A multiscale observational analysis, *Geophys. Res. Lett.*, *39*, L21707, doi:10.1029/2012GL053703.

Miralles, D. G., A. J. Teuling, C. C. van Heerwaarden, and J. Vilà-Guerau de Arellano (2014), Mega-heatwave temperatures due to combined soil desiccation and atmospheric heat accumulation, *Nat. Geosci.*, *7*(5), 345–349, doi:10.1038/ngeo2141.

Morice, C. P., J. J. Kennedy, N. A. Rayner, and P. D. Jones (2012), Quantifying uncertainties in global and regional temperature change using an ensemble of observational estimates: The HadCRUT4 data set, *J. Geophys. Res.*, *117*, D08101, doi:10.1029/2011JD017187.

Mueller, N. D., E. E. Butler, K. A. McKinnon, A. Rhines, M. Tingley, N. M. Holbrook, and P. Huybers (2015), Cooling of US Midwest summer temperature extremes from cropland intensification, *Nat. Clim. Change*, *6*(3), 317–322, doi:10.1038/nclimate2825.

Orlowsky, B., and S. I. Seneviratne (2012), Global changes in extreme events: Regional and seasonal dimension, *Clim. Change*, *110*, 669–696, doi:10.1007/s10584-011-0122-9.

Palmer, T. (2014), Build high-resolution global climate models, *Nature*, *515*, 338–339.

Portmann, R. W., S. Solomon, and G. C. Hegerl (2009), Spatial and seasonal patterns in climate change, temperatures, and precipitation across the United States, *Proc. Natl. Acad. Sci. U.S.A.*, *106*(18), 7324–7329, doi:10.1073/pnas.0808533106.

Quesada, B., R. Vautard, P. Yiou, M. Hirschi, and S. I. Seneviratne (2012), Asymmetric European summer heat predictability from wet and dry southern winters and springs, *Nat. Clim. Change*, *2*(10), 736–741, doi:10.1038/nclimate1536.

Rhines, A., and P. Huybers (2013), Frequent summer temperature extremes reflect changes in the mean, not the variance, *Proc. Natl. Acad. Sci. U.S.A.*, *110*(7), E546–E546, doi:10.1073/pnas.1218748110.

Screen, J. A., and I. Simmonds (2013), Exploring links between Arctic amplification and mid-latitude weather, *Geophys. Res. Lett.*, *40*, 959–964, doi:10.1002/grl.50174.

Seneviratne, S. I., D. Lüthi, M. Litschi, and C. Schär (2006), Land–atmosphere coupling and climate change in Europe, *Nature*, *443*(7108), 205–209, doi:10.1038/nature05095.

Seneviratne, S. I., T. Corti, E. L. Davin, M. Hirschi, E. B. Jaeger, I. Lehner, B. Orlowsky, and A. J. Teuling (2010), Investigating soil moisture–climate interactions in a changing climate: A review, *Earth Sci. Rev.*, *99*(3–4), 125–161, doi:10.1016/j.earscirev.2010.02.004.

Seneviratne, S. I., et al. (2013), Impact of soil moisture-climate feedbacks on CMIP5 projections: First results from the GLACE-CMIP5 experiment, *Geophys. Res. Lett.*, *40*, 5212–5217, doi:10.1002/grl.50956.

Seneviratne, S. I., M. G. Donat, A. J. Pitman, R. Knutti, and R. L. Wilby (2016), Allowable CO_2 emissions based on regional and impact-related climate targets, *Nature*, *529*(7587), 477–483, doi:10.1038/nature16542.

Sillmann, J., V. V. Kharin, F. W. Zwiers, X. Zhang, and D. Bronaugh (2013), Climate extremes indices in the CMIP5 multimodel ensemble: Part 2. Future climate projections, *J. Geophys. Res. Atmos.*, *118*, 2473–2493, doi:10.1002/jgrd.50188.

Taylor, K. E., R. J. Stouffer, and G. A. Meehl (2012), An overview of CMIP5 and the experiment design, *Bull. Am. Meteorol. Soc.*, *93*(4), 485–498, doi:10.1175/BAMS-D-11-00094.1.

Thiery, W., E. L. Davin, D. M. Lawrence, A. L. Hirsch, M. Hauser, and S. I. Seneviratne (2017), Present-day irrigation mitigates heat extremes, *J. Geophys. Res. Atmos.*, *122*, 1403–1422, doi:10.1002/2016JD025740.

Vasseur, D. A., J. P. Delong, B. Gilbert, H. S. Greig, C. D. G. Harley, K. S. Mccann, V. Savage, T. D. Tunney, and M. I. O'Connor (2014), Increased temperature variation poses a greater risk to species than climate warming, *Proc. R. Soc. B*, *281*, doi:10.1098/rspb.2013.2612.

Vogel, M. M., R. Orth, F. Cheruy, S. Hagemann, R. Lorenz, B. J. J. M. van den Hurk, and S. I. Seneviratne (2017), Regional amplification of projected changes in extreme temperatures strongly controlled by soil moisture-temperature feedbacks, *Geophys. Res. Lett.*, *44*, 1511–1519, doi:10.1002/2016GL071235.